SCIENCE CHINA
Earth Sciences

• RESEARCH PAPER •

August 2011 Vol.54 No.8: 1206–1214
doi: 10.1007/s11430-011-4212-3

Feature analysis of LIDAR waveforms from forest canopies

LIU QingWang, LI ZengYuan*, CHEN ErXue, PANG Yong, LI ShiMing & TIAN Xin

State Laboratory for Forest Remote Sensing and Information Techniques, Research Institute of Forest Resource Information Techniques of Chinese Academy of Forestry, Beijing 100091, China

Received April 27, 2010; accepted December 6, 2010; published online June 21, 2011

Airborne light detection and ranging (LIDAR) can detect the three-dimensional structure of forest canopies by transmitting laser pulses and receiving returned waveforms which contain backscatter from branches and leaves at different heights. We established a solid scatterer model to explain the widened durations found in analyzing the relationship between laser pulses and forest canopies, and obtained the corresponding rule between laser pulse duration and scatterer depth. Based on returned waveform characteristics, scatterers were classified into three types: simple, solid and complex. We developed single-peak derivative and multiple-peak derivative analysis methods to retrieve waveform features and discriminate between scatterer types. Solid scatterer simulations showed that the returned waveforms were widened as scatterer depth increased, and as space between sub-scatterers increased the returned waveforms developed two peaks which subsequently developed into two separate sub-waveforms. There were slight differences between the durations of simulated and measured waveforms. LIDAR waveform data are able to describe the backscatter characteristics of forest canopies, and have potential to improve the estimation accuracy of forest parameters.

remote sensing, forest canopy, LIDAR, waveform feature, solid scatterer

Citation: Liu Q W, Li Z Y, Chen E X, et al. Feature analysis of LIDAR waveforms from forest canopies. Sci China Earth Sci, 2011, 54: 1206−1214, doi: 10.1007/ s11430-011-4212-3

Forest canopies are considered a structurally complex sub-ecosystem with many ecologically critical functions, such as rainfall interception, light absorption, uptake of gases and provision of wildlife habit [1]. Canopy structure is the spatio-temporal organization of aboveground vegetation components [2], and difficulties in canopy access have in the past imposed severe limitations on the quantification of canopy structure [3]. Light detection and ranging (LIDAR) technology has developed rapidly in recent years and has strong potential for characterizing forest canopy structure [4–6].

LIDAR is an active remote sensing technique, and can measure precisely terrain and its features by transmitting laser pulses and receiving returned energy [7, 8]. For forest canopies, the penetrability of laser pulses is caused mainly by gaps among leaves and branches. When the laser pulse reaches the forest canopy surface, a portion of the energy is back-scattered the sensor and the residual energy penetrates the rest of the canopy and can reach the ground. LIDAR has been used to reconstruct canopy structures such as tree height, crown diameter and stem density, which are important for environmental modeling [9–11].

Current studies on LIDAR waveform data processing can usually fall into two groups: waveform simulation and waveform decomposition. Waveform simulation models the interactive relationship between laser pulses and vegetation. Sun et al. [12] developed a LIDAR waveform simulation model and found that the slower observed decay of measured waveforms than simulated waveforms might indicate the existence of understories, and also suggest that higher-

*Corresponding author (email: lizy@caf.ac.cn)

order scattering from the upper canopy might contribute to the LIDAR signals. Ni-Meister et al. [13] investigated the relationship between laser waveforms and canopy structure parameters, and the effects of the spatial arrangement of canopy structure on this relationship, through a modified geometric optical and radiative transfer (GORT) model. Their simulation showed that vegetation clumping caused a larger gap probability and smaller waveforms.

Waveform decomposition has been used to extract waveform features of different scatterers to improve the estimation accuracy of forest parameters. Hofton et al. [14] assumed each component of waveform was described by a Gaussian function, which were decomposed using a nonnegative least-squares method (LSM) optimized with the Levenburg-Marquardt method. Persson et al. [15] decomposed waveforms using the Expectation Maximization (EM) algorithm, which could extract more points compared with the real time processing echo extracted by LIDAR system. Wagner et al. [8] assumed the returned waveforms was made up of a series of Gaussian pulses, and provided the range, amplitude, and width for each pulse by Gaussian decomposition. Mallet et al. [11] reviewed the waveform data processing methods and their applications, and found that current studies utilized only part of the information extracted from full waveform data. They concluded that more research was required to further extract waveform information.

We observed the duration (i.e. the interval between the start and and time of a pulse) of returned waveforms was longer than transmitted pulses through analysis of the interactive relationship between laser pulses and forest canopies. This phenomenon has not been discussed in the literature about waveform data processing. The complex three-dimensional forest structure is required for waveform simulations based on the GORT model [12, 13]. In this study we use a simplified canopy structure scheme to derive a solid scatterer LIDAR model. We define the corresponding relationship between duration variations and forest canopy spatial characteristics by analyzing the effect of time-variable transmitted pulses on the returned waveforms. Finally, we develop new methods of waveform feature extraction based on initial feature analysis of different scatterer waveforms to improve the estimation accuracy of forest canopy parameters.

1 Theory

LIDAR operates on basic principles similar to conventional radio detection and ranging (RADAR), but LIDAR uses very short wavelengths and has higher accuracy and resolution [16]. According to electromagnetic propagation, the RADAR range equation is applied equally to LIDAR as shown in eq. (1):

$$P_{\mathrm{R}} = \frac{P_{\mathrm{T}} D^2}{4\pi R^4 \beta_{\mathrm{T}}^2} \cdot \sigma \cdot \mu_{\mathrm{SYS}} \cdot \mu_{\mathrm{ATM}},\ \sigma = \frac{4\pi}{\Omega_{\mathrm{S}}} \rho A_{\mathrm{S}}, \tag{1}$$

where P_{R} is the received signal power, P_{T} is the transmitter power, D is the aperture diameter of the receiver optics, R is the sensor distance to target, β_{T} is the transmitter beam width, σ is the backscatter cross-section, Ω_{S} is the scattering solid angle, ρ is the scatterer reflectivity, A_{S} is the receiving area of the scatterer, μ_{SYS} is the system transmission factor, and μ_{ATM} the atmospheric transmission factor.

The transmitted laser pulse energy is characterized by a single peak varying with time. The returned backscatter energy has either single or multiple peaks depending on scatterer structure. Scatterers are classified as simple, solid or complex depending on the spatial distribution of backscatter cross-section profiles. Simple scatterers, such as points or planes perpendicular to the pulse direction, directly scatter transmitted pulses without widening pulse durations. The returned energy received by the sensor is calculated as [8]:

$$P_{\mathrm{R}}(t) = \frac{D^2}{4\pi R^4 \beta_{\mathrm{T}}^2} \cdot P_{\mathrm{T}}(t - T_{\mathrm{T}}) \cdot \sigma \cdot \mu_{\mathrm{SYS}} \cdot \mu_{\mathrm{ATM}},\ T_{\mathrm{T}} = \frac{2R}{c}, \tag{2}$$

where t is the time, T_{T} is the time delay, c is the light velocity.

For solid scatterers such as forest canopy, transmitted pulses are intercepted by different leaves and branches along the pulse direction. The returned signal is a combination of backscatters returned at different times. To analyze properties of solid scatterers, it is assumed that the solid scatterer is a collection of multiple-layered sub-scatterers. Each single sub-scatterer is assumed to be a simple scatterer, and the distance between layers is assumed to be the same. The backscatter cross-sections of n layers are denoted σ_1, σ_2,…σ_n. Similarly, the transmitted pulse is divided into m layers, and the time intervals between layers are considered equal. The transmitted energies from layers are denoted $P_{\mathrm{T}1}$, $P_{\mathrm{T}2}$,…$P_{\mathrm{T}m}$ from the start to end time of the transmitted pulse. The corresponding relationship between the distance interval Δr and the time interval Δt is

$$\Delta r = \frac{1}{2} c \cdot \Delta t. \tag{3}$$

Figure 1 is a diagrammatic representation of a solid scatterer. The transmitted pulse duration is T_{L}, the start time is $t_{\mathrm{L}1}$, the end time is t_{Lm}, the distance between the sensor and the top of the target is R_{T}, the round-trip travel duration between the sensor and the top of the target is T_{T}, the travel time of the pulse start point arriving at the top of the target is t_{R1}, the travel time of the pulse start point transmitted from the top to the floor and back again is t_{Rn}, the round-trip travel duration through the target is T_{R}, and the scatterer depth is R_{R}.

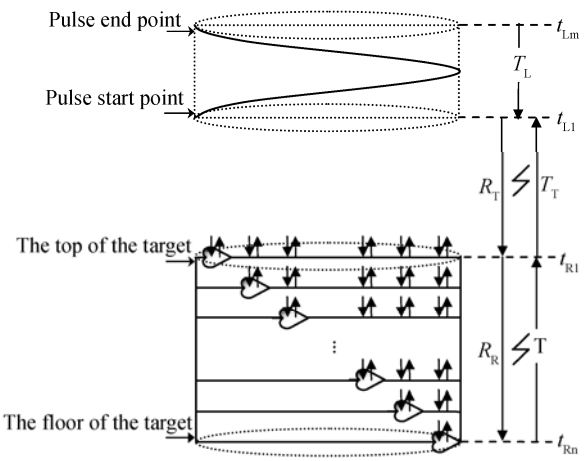

Figure 1 Diagrammatic representation of a solid scatterer. Annotations are described in the text.

Next, let us consider the energy scattered by the first target layer. At time t_{R1} the part of the energy P_{T1} scattered directly by σ_1 is denoted $P_1\sigma_1$, and the residual energy of P_{T1} penetrates to the deeper layers. P_{T2} to P_{Tm} do not scatter due to not reaching the target. Here we do not consider attenuation by the LIDAR system and the atmosphere on the transmitted pulse energy. The radiation energy at the top of the target is P_{R1} (i.e. $P_1\sigma_1$), where

$$P_{R1} = \frac{D^2}{4\pi R_T^4 \beta_T^2} \cdot P_{T1} \cdot \sigma_1. \quad (4)$$

At time t_{R2}, the part of the energy P_{T2} scattered directly by σ_1 is denoted $P_2\sigma_1$, and the residual energy of P_{T2} penetrates to the deeper layers. The part of the residual energy of P_{T1} backscattered to the top of the target by σ_2 is denoted $P_1\sigma_2$. A part of the residual P_{T1} energy reaches σ_3 without back scatter. The other part of the residual P_{T1} energy penetrates to the deeper layers. The radiation energy at the top of the target is P_{R2} (i.e. $P_2\sigma_1 + P_1\sigma_2$) where

$$P_{R2} = \frac{D^2}{4\pi R_T^4 \beta_T^2} \cdot P_{T2} \cdot \sigma_1 + \frac{D^2}{4\pi (R_T + R_{R1})^4 \beta_T^2} \cdot P_{T1} \cdot \sigma_2. \quad (5)$$

The variable R_R can be neglected in situations where $R_R << R_T$. Eq. (5) is approximated to

$$P_{R2} = \frac{D^2}{4\pi R_T^4 \beta_T^2} \cdot (P_{T2} \cdot \sigma_1 + P_{T1} \cdot \sigma_2). \quad (6)$$

By analogy, the discrete function of radiant energy at the top of the target that varies with time is

$$P_R(t) = \frac{D^2}{4\pi R_T^4 \beta_T^2} \sum_{i=0}^{(t-T_T)/\Delta t} P_T(t - T_T - i \cdot \Delta t) \cdot \sigma(i \cdot \Delta t). \quad (7)$$

Assuming that the energy of transmitted pulses and backscatter cross-section profiles are continuous distributions, the integral form of eq. (7) is expressed as

$$P_R(t) = \frac{D^2}{4\pi R_T^4 \beta_T^2} \cdot \int_{T_T}^{T_T+T_R+T_L} P_T(t - T_T - \tau) \cdot \sigma(\tau) \cdot \mathrm{d}\tau. \quad (8)$$

Eq. (8) can be simplified subsequently to

$$P_R(t) = \frac{D^2}{4\pi R_T^4 \beta_T^2} \cdot [P_T(t - T_T) * \sigma(t)], \quad (9)$$

where * is the convolution operator.

We divided the scatterer into n layers according to eq. (3). If the distance interval is doubled, the scatterer is divided into $n/2$ layers. The energy scattered by the top of the target will alternate with transmitted energy interacting alternately with odd and even target layers. Eq. (7) can then change into the form:

$$P_R(t) = \begin{cases} \dfrac{D^2}{4\pi R_T^4 \beta_T^2} \displaystyle\sum_{i=0}^{(t-T_T)/\Delta t} P_T[t - T_T - (2i+1) \cdot \Delta t] \cdot \sigma'(i \cdot \Delta t) \\ \dfrac{D^2}{4\pi R_T^4 \beta_T^2} \displaystyle\sum_{i=0}^{(t-T_T)/\Delta t} P_T(t - T_T - 2i \cdot \Delta t) \cdot \sigma'(i \cdot \Delta t), \end{cases} \quad (10)$$

where $2i$+1 is the odd layer, $2i$ is the even layer.

If the scatterer distance interval increases or decreases, eq. (7) will change into another form. This reflects that the energy scattered theoretically by the target varies with the distance and time intervals.

The laser energy is in fact distributed unevenly in the illuminated area, and decreases sharply from the center to the edge. The energy density distribution function $D(r)$ of the illuminated area is defined at the footprint center of the laser pulse. The backscatter cross-section is weighted with $D(r)$ according to the spatial position, and becomes $\sigma_W(t, r)$:

$$\sigma_W(t, r) = D(r) \circ \sigma(t, r), \quad (11)$$

where r is the radius from the center to the edge of the pulse footprint. We substitute $\sigma(t)$ in eq. (9) with $\sigma_W(t, r)$ and obtain

$$P_R(t) = \frac{D^2}{4\pi R_T^4 \beta_T^2} \cdot [P_T(t - T_T) * \sigma_W(t, r)]. \quad (12)$$

Considering the attenuation effect of LIDAR system and atmosphere on the transmitted pulse energy, the calibrated result is

$$P_R(t) = \frac{D^2}{4\pi R_T^4 \beta_T^2} \cdot [P_T(t - T_T) * \sigma_W(t, r)] \cdot \eta_{SYS} \cdot \eta_{ATM}. \quad (13)$$

For complex scatterers, such as canopies with multiple clusters, each cluster can be considered a simple or solid scatterer within the entire scattering space, in which the

distance between clusters is generally greater than the distance corresponding to the transmitted pulse duration. The LIDAR equation for a complex scatterer is expressed simply as the addition of simple and solid scatterers:

$$P_{\mathrm{R}}(t) = \sum_i P_{\mathrm{R},i}(t) + \sum_j P_{\mathrm{R},j}(t), \tag{14}$$

where $P_{\mathrm{R},i}(t)$ is the energy from the simple scatter, and $P_{\mathrm{R},j}(t)$ is the energy from the solid scatterer.

2 Methods

2.1 Waveform feature analysis

The LIDAR system records the energy distribution (i.e. waveforms) of transmitted pulses and backscatter signals from targets. The scatterers are classified as simple, solid or complex by analyzing waveform features, such as the start point, peak and end point, from which the scatterer features can be obtained.

An example of waveform features is shown in Figure 2. The left panel shows the transmitted waveform, and the right panel shows the returned waveform. The horizontal axes are the sampling time of pulses with 1 ns intervals, and the vertical axes are the relative intensity.

(1) Waveform features of the simple scatterer. A simple scatterer has one returned waveform, which can be regarded as being reduced in proportion to the energy of the original transmitted pulse. The duration T_{LR} of the returned waveform equals the duration T_{LT} of the transmitted waveform according to the simple scatterer equation. T_{LR} and T_{LT} are obtained from the start and end points of the waveform. Considering the noise threshold of the LIDAR detector, T_{LR} is always less than T_{LT}. Therefore T_{LT} needs to be modified so that the energy of the transmitted waveform is reduced to the same level as the energy of the returned waveform.

There are three methods to obtain the distance between the simple scatterer and sensor. The first distance is calculated by the time difference T_{TR} of the start points between the transmitted and returned waveforms. The second distance is calculated by the time difference T_{TD} of the end points between the transmitted and returned waveforms. The third distance is calculated by the time difference T_{TP} of the peaks between the transmitted and returned waveforms. The first and second distances need to be modified for noise effects. The third distance is concerned only with the resolution of the time recorder, and does not need to account for noise effects.

(2) Waveform features of the solid scatterer. A typical solid scatterer has an widened returned waveform, the value of which is determined by the depth of the scatterer. The relationship between the returned waveform duration T_{LR} and the transmitted waveform duration T_{LT} is

$$T_{\mathrm{LR}} = T_{\mathrm{LT}} + T_{\mathrm{R}}. \tag{15}$$

The distance R_{TR} between the top of the solid scatterer and the sensor is calculated by the time difference T_{TR} of the start points between the transmitted and returned waveforms. The distance R_{TD} between the floor of the solid scatterer and the sensor is calculated by the time difference T_{TD} of the end points between the transmitted and returned waveforms. The distance R_{TP} between a given point within the solid scatterer and the sensor is calculated by the time difference T_{TR} of the peaks between the transmitted and returned

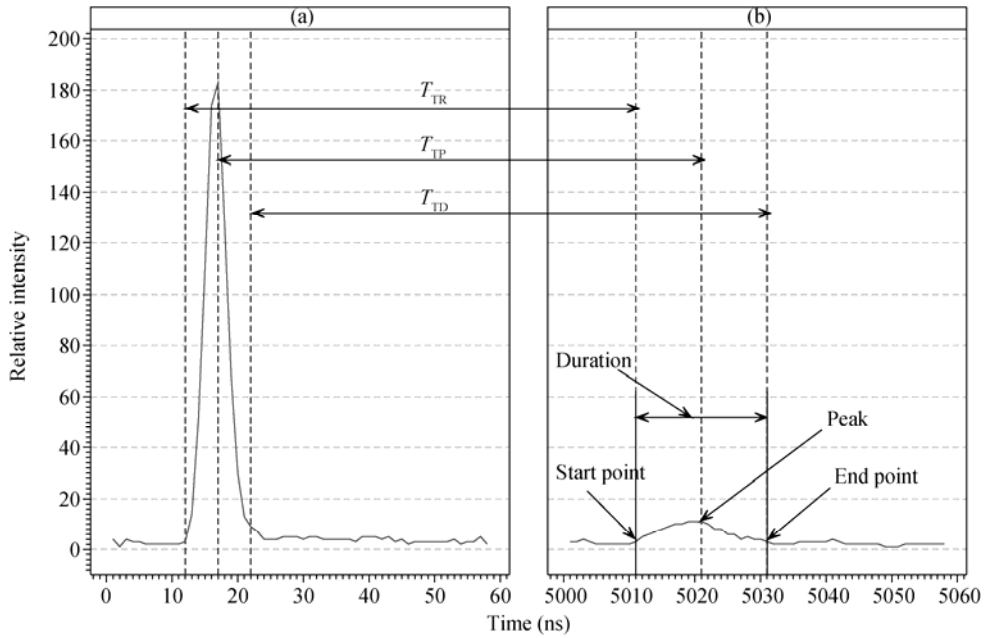

Figure 2 Example of LIDAR waveform features. (a) Transmitted waveform; (b) returned waveform.

waveforms. The scatterer depth is calculated by the difference between R_{TD} and R_{TR}. The transmitted waveform should be modified due to the effect of noise.

(3) Waveform features of the complex scatterer. The returned waveform of a complex scatterer has multiple peaks, which can be regarded as a combination of simple or solid scatterers. The number of peaks is detected by the energy distribution of the returned waveform. Each peak corresponds to a sub-waveform, the features of which are calculated to obtain all features of the complex scatterer.

2.2 Waveform feature recognition

There exists difference between features extracted from returned waveforms, which are divided usually into two classes according to peek characteristics. The first class is single-peak waveforms corresponding to simple and solid scatterers, from which we can directly extract the related waveform features. The second class is multiple-peak waveforms corresponding to complex scatterers, from which we can get sub-waveforms and their features by waveform decomposition algorithms, or we can extract directly the waveform features using a simplified algorithm.

The threshold algorithm is the simplest method of waveform feature recognition. The noise level is used to determine the threshold. If the returned waveform energy is less than the threshold, it is set to zero, otherwise it remains unchanged. For single-peak waveforms, the non-zero start position is used as the waveform start point, the non-zero end position is used as the end point, and the maximum energy as the peak. For multiple-peak waveforms, the returned waveform is divided into several segments which correspond to clusters. The non-zero start position of each segment is used as the start point of each sub-waveform, the non-zero end position is used as the end point, and the maximum energy as the peak. The algorithm is simple, easy to implement, and efficient. Its shortcoming is that the waveform start and end points are influenced easily by the threshold. This means the duration will be shortened erroneously if the threshold is too large, and that if the threshold is too small, some waveform peaks will be misjudged as single peek.

The waveform decomposition algorithm remedies the defect of threshold algorithm, and can extract sub-waveforms to a certain extent, but it is more complex and less efficient. Therefore we developed compromisely two algorithms of waveform feature recognition: a single-peak derivative (SPD) and multiple-peak derivative (MPD). The SPD was used to recognize quickly the maximum peak features of the returned waveform. The MPD was used to recognize the features of all peaks of the returned waveform.

The SPD first identifies the maximum energy in the returned waveform, and then calculates the first-order derivative from the maximum to the start point. If there are N non-zero values in series identified above the noise threshold, the rising edge has been located. The SPD keeps searching in the start point direction. If the energy is less than the threshold or the derivative is negative, this indicates that the start point has been reached. Finally, the SPD calculates the first-order derivative from the maximum to the end point. If there are N non-zero values in series identified above the noise threshold, the falling edge has been located. The SPD keeps searching to the end point. If the energy is less than the threshold or the derivative is negative, this indicates that the end point has been reached. The SPD algorithm is easy to implement, and overcomes the shortcoming of the threshold algorithm. The SPD algorithm identifies the maximum peak of the returned waveform, but fails to identify other peaks of the multiple-peak waveform.

The MPD calculates the first-order derivative from the start to the end positions of the returned waveform. If there are N positive values in series identified above the noise threshold, the rising edge has been found. The MPD records the corresponding start point (i.e. the first positive value position in N), keeps searching, and records the maximum energy position. If there are N non-zero values in series identified above the noise threshold, the falling edge has been identified. The MPD keeps searching to the end point. If the energy is less than the threshold or the derivative is negative, this indicates that the end point has been reached, and the first sub-waveform identified. The MPD searches until all sub-waveforms are found. This algorithm overcomes the disadvantage of the SPD, but is less efficient. The difference to the SPD is the criteria for identifying the rising edge of the returned waveform, which is used to overcome the effect of the noise threshold on identifying the start point of the returned waveform. However the MPD is itself problematic because the first-order derivatives of the rising edge of some waveforms do not have N positive values in series. This can lead to failure in features recognition, which the SPD could be used to address.

The range of N values in the SPD and MPD is from 1 to the integer of time length at the height of median energy (HOME) of the transmitted pulse. The SPD and MPD algorithms can eliminate the effect of energy fluctuations caused by detection noise, and retain waveform rising and falling edge features when the N value is maximum (N is 3 for the test site; see below).

In order to discriminate between scatterer types, we first used the MPD to extract returned waveform features and identify the presence of either single or multiple peaks. If the returned waveform has a single peak, the scatterer is either simple or solid depending on the relationship between the duration of returned waveform and the duration of transmitted pulse. If the waveform has multiple peaks, the scatterer is complex. The SPD can be used to extract waveform features when the MPD fails to do so, and the discrimination of scatterer type is similar to single peak identification by the MPD.

3 Test site and data

3.1 Description of the test site

The test site is located at Xishui farm, Su'nan Yuguzu Autonomous County in the Gansu Qilian Mountains National Nature Reserve (100°15′E, 38°32′N). The site is a water resource conservation forest in the Dayekou Basin of the Qilian Mountains, and lies within the temperate alpine cold semiarid and semi-humid zone, characterized by mountain forest-steppe [17, 18]. Sunny slopes are covered with mountain grassland, and shady slopes are forested. The elevation ranges from 2700 to 3000 m above sea level, with mean elevation of ~2800 m. The area slopes are ~9° to the northeast. The forest cover is natural mature secondary forest dominated by *Picea crassifolia Kom.*, and the forest floor is covered mainly with moss.

3.2 Data from the test site

LIDAR data were acquired on June 23, 2008 by a LiteMapper 5600 system. The laser scanner was a Riegl LMS-Q560, laser wavelength was 1550 nm, pulse length was 3.5 ns, and laser beam divergence was 0.5 mrad. The average sampling distance was 0.54 m, i.e. 3.43 points m^{-2}. A field survey was conducted from June 1 to 13, 2008. A 1-ha plot was established on a hillside. Parameters of individual trees were measured such as diameter at breast height (DBH), tree height and crown diameter. Tree positions were recorded by differential global position system (DGPS) and total station.

4 Results and analysis

4.1 Waveform simulations

The energy of transmitted pulses varied with time, and was described by a Gaussian function [8]. We assumed that three standard deviations were 5 ns, the amplitude was 132 (relative intensity), and the energy attenuation coefficient (i.e. the ratio between returned and transmitted energy) was 0.2.

The energy variations in returned waveforms were influenced strongly by backscatter cross-sections. The returned waveform simulations of simple scatterers were quite simple. So, we simulated the returned waveforms of solid scatterers, and assumped that the backscatter cross-seciotn had a normal distribution, the distance interval was 0.15 m, and the corresponding round-trip time interval was 1 ns. Figure 3 shows a set of simulations of returned waveforms from scatterers with increasing depths. The returned waveforms widened gradually and the peak intensities decreased gradually.

The returned waveforms also changed with the distances between sub-scatterers. The returned waveforms were slightly widened with increasing distance, two peaks began to appear at a distance of 0.6 m, and then became two individual sub-waveforms at 1.5 m (Figure 4).

4.2 Comparisons between waveform features

We used the SPD to extract features of returned waveforms, which were used to build the simple or solid scatterers. The simulated waveforms can be obtained from the model using

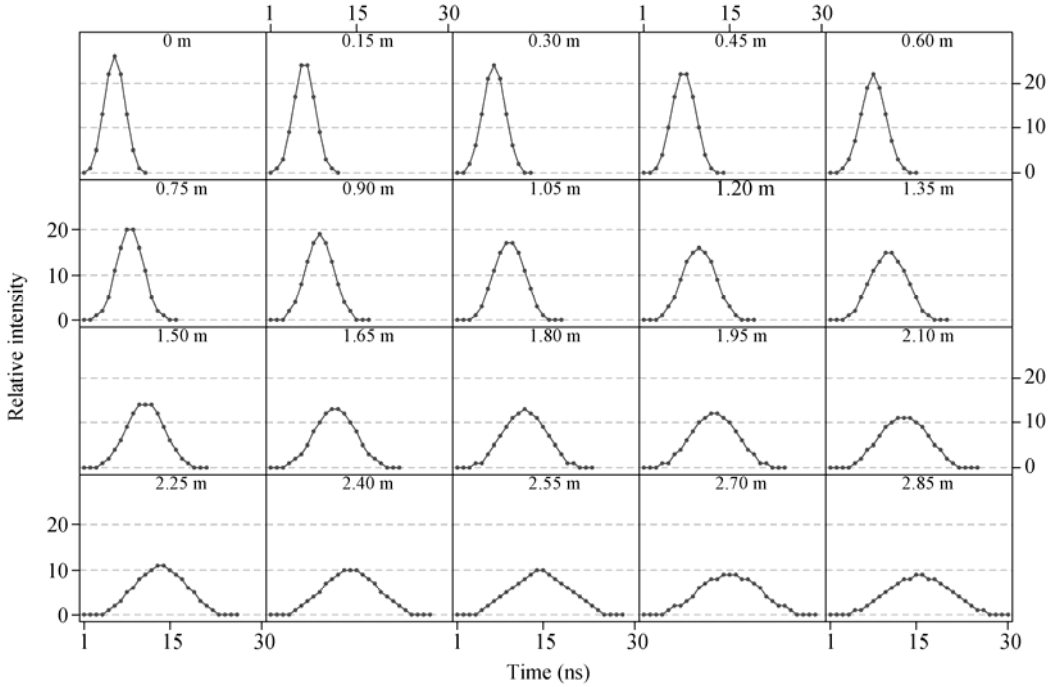

Figure 3 Returned waveforms from scatterers with increasing depths.

measured waveforms and simulated solid scatterers. The SPD was used to extract features of simulated waveforms, which were then compared with features of measured waveforms. The durations of simulated waveforms were on average ~2 ns less than those of measured waveforms, and the durations of the rising and falling edges were reduced by ~1 ns (Figure 5).

We used the MPD to extract the features of returned waveforms, which were used to build the complex scatterers. The simulated waveforms were obtained from the model, and were then compared with those of the measured waveforms. Some sub-waveforms with small intensities were not recognized because their energies fluctuated around the noise level (Figure 6). This may be due to multiple scatter-

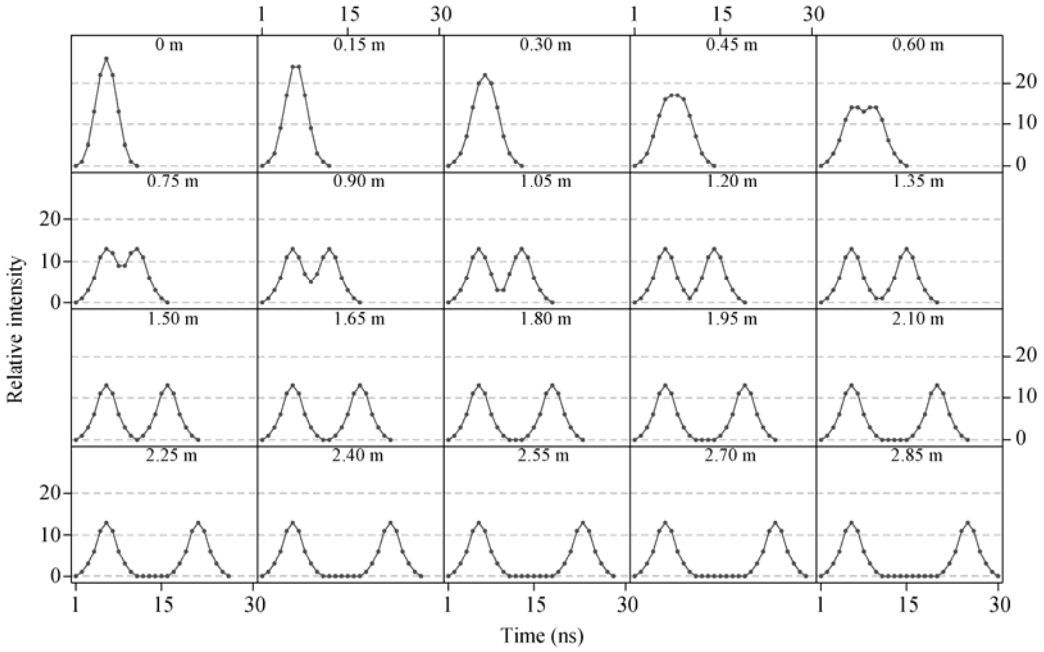

Figure 4 Returned waveforms from scatterers with increasing distances between sub-scatterers.

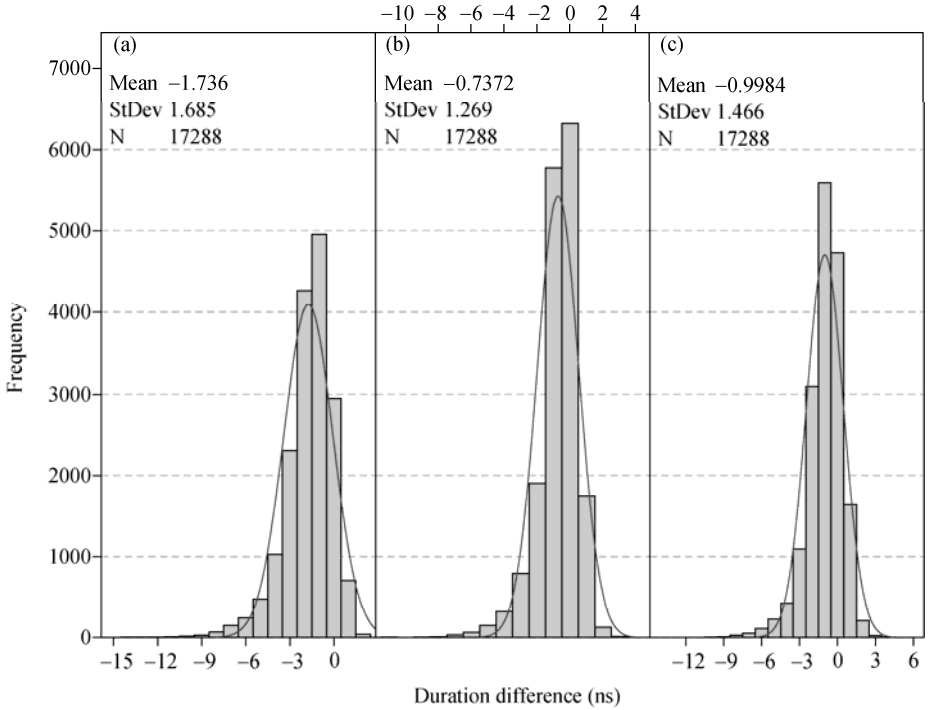

Figure 5 Histograms of the differences between measured and simulated waveform durations. (a) Differences for full waveform durations; (b) differences for rising edge durations; (c) differences for falling edge durations.

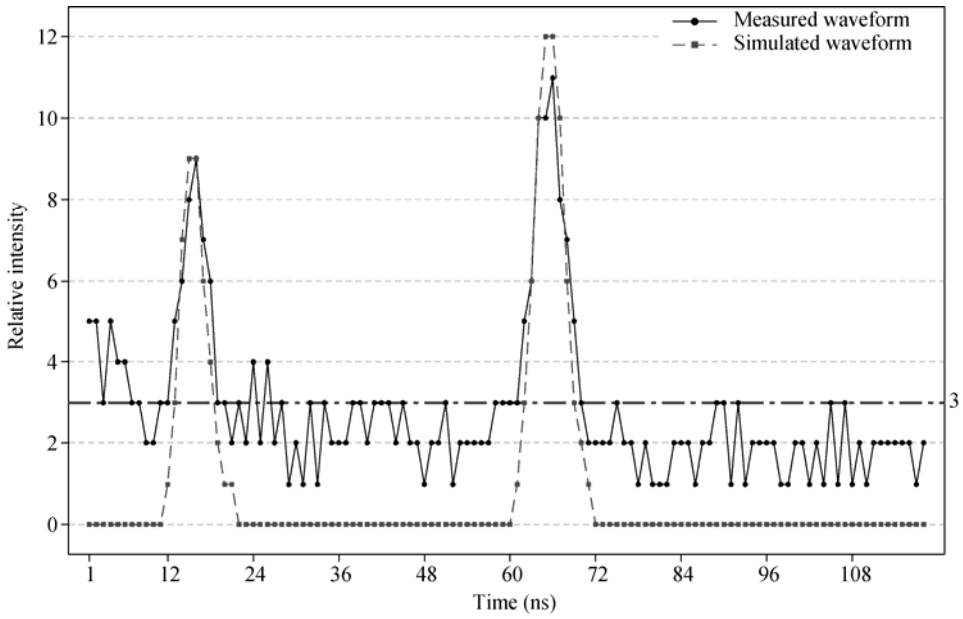

Figure 6 Simulated and measured waveforms of a complex scatterer.

ing or low vegetation scattering, which were not taken into account in the waveform simulations.

5 Discussion and conclusions

The distance intervals between solid scatterer layers should match the time intervals between the transmitted pulse layers. The time interval corresponds generally to the distance interval round-trip travel time. The simulated waveform decreases from partially losing energy if the distance interval is too large or too small, which would decrease the effective backscatter cross-section profiles. Appropriate distance interval in the simulations based on time interval should be established to simulate accurately the returned waveforms.

The LIDAR equations describing different scatterers were essentially correlated. The scatterers transform into each other under particular conditions during simulation of returned waveforms. The solid scatterers changed into simple scatterers if the scatterer depth was less than the distance interval, and the returned waveform widened with increasing scatterer depth. With increasing distance between two sub-scatterers, the returned waveform developed two peaks that subsequently differentiated into individual sub-waveforms, indicating the transformation from a solid to a complex scatterer.

Our waveform simulation considered only single scattering, and neglected the effect of low vegetation on waveform feature recognition. This contributed to errors in the simulated waveforms using these recognized features, and the detection errors for waveform rising and falling edges may be one time interval taking into account the effect of noise.

The SPD and MPD detected rapidly scatterer waveform features, but obtained only a coarse distribution for backscatter cross-section profiles. The extraction of higher-resolution backscatter cross-section profiles may be achieved by the application of more sophisticated waveform analysis methods such as Gaussian decomposition and waveform deconvolution.

The backscatter cross-section profiles obtained by our waveform feature analysis can be used in conjunction with other remote sensing data to better estimate forest parameters, to verify coarse-resolution remote sensing data, and be used in the development of coupled models to improve the estimation accuracy of regional-scale forest parameters.

We are grateful to persons participating in data acquisition and preprocessing for the Watershed Allied Telemetry Experimental Research (WATER) program. This work was supported by the National Basic Research Program of China (Grant No. 2007CB714404), the Central Public-Interest Scientific Institution Basal Research Fund of China (Grant No. IFRIT 200803), and the National Hi-Tech Research and Development Program of China (Grant No. 2009AA12Z1461).

1 Nadkarni D M, Parker G G, Rinker H B, et al. The nature of forest canopies. In: Lowman D M, Rinker H B, eds. Forest Canopies. 2nd ed. San Diego: Elsevier Academic Press, 2004. 3–23
2 Parker G G. Structure and microclimate of forest canopies. In: Lowman M D, Nadkarni N M, eds. Forest Canopy. San Diego: Academic Press, 1995. 73–106
3 Lowman D M, Nadkarni N M. Canopy access techniques. In: Lowman M D, Nadkarni N M, eds. Forest Canopy. San Diego: Academic Press, 1995. 3–25
4 Lefsky M A, Cohen W B, Acker S A, et al. Lidar remote sensing of the canopy structure and biophysical properties of Douglas-Fir Western Hemlock Forests. Remote Sens Environ, 1999, 70: 339–361
5 Brandtberg T, Warner T A, Landenberger R E, et al. Detection and analysis of individual leaf-off tree crowns in small footprint, high

sampling density lidar data from the eastern deciduous forest in North America. Remote Sens Environ, 2003, 85: 290–303
6 Popescu S C, Zhao K. A voxel-based lidar method for estimating crown base height for deciduous and pine trees. Remote Sens Environ, 2008, 112: 767–781
7 Baltsavias E P. Airborne laser scanning: Basic relations and formulas. ISPRS-J Photogr Remote Sens, 1999, 54: 199–214
8 Wagner W, Ullrich A, Ducic V, et al. Gaussian decomposition and calibration of a novel small-footprint full-waveform digitising airborne laser scanner. ISPRS-J Photogr Remote Sens, 2006, 60: 100–112
9 Drake J B, Weishampel J F. Simulating vertical and horizontal multifractal patterns of a longleaf pine savanna. Ecol Model, 2001, 145: 129–142
10 Lefsky M A, Hudak A T, Cohen W B, et al. A Patterns of covariance between forest stand and canopy structure in the Pacific Northwest. Remote Sens Environ, 2005, 95: 517–531
11 Mallet C, Bretar F. Full-waveform topographic lidar: State-of-the-art. ISPRS-J Photogr Remote Sens, 2009, 64: 1–16
12 Sun G, Ranson K J. Modeling LIDAR returns from forest canopies. IEEE Trans Geosci Remote Sensing, 2000, 38: 2617–2626
13 Ni-Meister W, Jupp D L B, Dubayah R. Modeling lidar waveforms in heterogeneous and discrete canopies. IEEE Trans Geosci Remote Sensing, 2001, 39: 1943–1958
14 Hofton M A, Minster J B, Blair J B. Decomposition of laser altimeter waveforms. IEEE Trans Geosci Remote Sensing, 2000, 38: 1989–1996
15 Persson Å, Söderman U, Töpel J, et al. Visualization and analysis of full-waveform airborne laser scanner data. International Archives of Photogrammetry. Remote Sens Spatial Inf Sci, 2005, 36: 103–108
16 Jelalian A V. Laser Radar Systems. London: Artech House, 1992. 1–57
17 Dang H, Zhao Y, Chen X. Law of the water transfer process of water-conversation forest in Qilian Mountains. Chin J Eco Agri, 2004, 12: 43–46
18 Ma Y, Wang J, Liu X, et al. Status of forestry ecosystem and protection countermeasure in the protection areas in Qilian Mountains. J Northwest Forest Univ, 2005, 20: 5–8